Eur. Phys. J. Special Topics **220**, 185–194 (2013)

DOI: 10.1140/epjst/e2013-01806-3

THE EUROPEAN PHYSICAL JOURNAL SPECIAL TOPICS

Regular Article

Modeling and numerical approximations for bubbles in liquid metal

Sebastian Aland[1,a], Stephan Schwarz[2], Jochen Fröhlich[2], and Axel Voigt[1]

[1] Institut für Wissenschaftliches Rechnen, 01062 TU Dresden, Germany
[2] Institut für Strömungsmechanik, 01062 TU Dresden, Germany

Received 17 December 2012 / Received in final form 5 February 2013
Published online 26 March 2013

Abstract. In simulations of liquid metals, various model approximations, each of which justified by experimental results lead to a simplified two-phase flow problem. This paper discusses numerical justifications for these approaches and provides quantitative results for a single rising bubble as a benchmark. Representing a bubble as a rigid object is shown to be valid for low Eötvös numbers in contaminated systems. Qualitative differences can be observed for larger Eötvös numbers. Further simulations are undertaken with different ratios of inner and outer viscosity. The benchmark problem considered may also be interesting for more general applications.

1 Introduction

Numerical simulation of two-phase flow problems with two immiscible fluids is a rapidly evolving field with numerous schemes and methods proposed every year. Applications range from computer graphic animations almost indistinguishable from reality [1] to the simulation of cooling systems in nuclear power plants [2]. Various approximations are required to achieve these results, e.g. neglecting the flow field in one fluid phase, neglecting the curvature effects of the fluid-fluid interface, or not resolving the two phases at all and treating one of the phases implicitly. While such approximations are not crucial in computer graphics, they are of the utmost importance in technical applications if, for example, the safety of a nuclear power plant depends on it.

We will not consider all approximations made in two-phase flow problems, but concentrate on a specific application, serving as an example for justification of physical modelling and numerical approximations. The situation considered stems from metallurgical applications featuring liquid metals in which bubbles are injected to clean and stir the melt. Such gas-liquid systems are essentially two-phase flows. The simplest model involving two viscous fluids is:

$$\rho_i \left(\frac{\partial \mathbf{u}_i}{\partial t} + \mathbf{u}_i \cdot \nabla \mathbf{u}_i \right) = -\nabla p_i + \eta_i \Delta \mathbf{u}_i + \mathbf{F}_i, \qquad \nabla \cdot \mathbf{u}_i = 0, \quad \text{in} \quad \Omega_i, \tag{1}$$

[a] e-mail: sebastian.aland@tu-dresden.de

where Ω_i, for $i = 1$ or 2, denotes the domain of each fluid phase, the bubbles ($i = 1$) and the surrounding fluid ($i = 2$), with ρ_i, $\mathbf{u}_i$, p_i, η_i, $\mathbf{F}_i$ being the density, velocity, pressure, viscosity and body force in domain Ω_i respectively. If $\eta_i \neq 0, i = 1, 2$, the following jump conditions hold across the interface Σ separating the domains:

$$[\mathbf{u}]_\Sigma = \mathbf{0}, \quad [-p\mathbf{I} + \eta\mathbf{D}]_\Sigma \cdot \mathbf{n} = -\sigma\kappa\mathbf{n}, \tag{2}$$

where $[f]_\Sigma = f_1 - f_2$ denotes the jump in f across Σ, $\mathbf{I}$ is the identity tensor, $\mathbf{D} = \left(\nabla\mathbf{u} + \nabla\mathbf{u}^T\right)$, $\mathbf{n}$ is the normal vector to Σ pointing into Ω_2, σ is the surface tension, κ is the total curvature (positive for a sphere). Let $\Omega = \Omega_1 \cup \Sigma \cup \Omega_2$ and let $\Gamma = \partial\Omega$ denote the boundary of the fluid domain.

The application of interest, however, has some additional properties which might require modifications to the above model, which we will refer to as the original model. Liquid metals are prone to oxidation and laden with contaminants. Consequently, an oxide layer forms at the gas-liquid interface, and contaminants and inclusions agglomerate at the interface. The agglomeration of particles at the interface and its effect on the two-phase flow problem can be modeled and incorporated into the above equations. Such models have been considered in [3,4] and lead to complicated boundary conditions at the interface, including an elastic energy and a density field for the agglomerate. These models, however, are too costly to be used for applications in which the interaction of large numbers of bubbles is of interest. Therefore, instead of modeling the agglomeration directly, the situation can also be modeled by an effective surface tension [5] which then assumed to be constant.

When this surface tension is very large, e.g. for small bubbles, the bubble shape remains constant and the agglomerated particles at the surface result in an effective no-slip condition. It then appears possible to model the bubble as a solid object. This simplification is supported by the experimentally observed correspondence of the drag of a fully contaminated spherical bubble to that of a solid sphere [6,7]. In that case the boundary conditions change and instead of the jump conditions (2) in the original model, a no-slip condition at the bubble interface is employed to describe the resulting flow.

A variant of the model suitable for somewhat larger bubbles is obtained by retaining the no-slip condition, but relaxing the restriction of constant shape by determining the shape of the bubble as a function of the surrounding flow. One possibility is to compute the balance of forces at the interface and adjust the local curvature to obtain equilibrium, as presented elsewhere in this volume. For small to moderate changes in shape, an even more efficient variant is possible, in which the shape is determined by a correlation obtained from experimental data. The resulting model for this two-phase flow reduces the complexity of the problem drastically and allows for three-dimensional (3D) computations of large numbers of bubbles possibly interacting. Examples of such simulations are presented in [8,9]. Accounting for the contaminants and inclusions in liquid metals thus actually simplifies the model instead of making it more complicated.

But how useful is the model? What is the modeling error with respect to other approaches? We will consider these issues and compare the results with the original model (1)-(2) and an approach in which the agglomerates are modeled directly. We do this using the benchmark problem proposed in [10] featuring a single bubble in a two-dimensional (2D) cylindrical channel with Γ a solid wall and $\Sigma \cap \Gamma = \emptyset$, i.e. the bubble is not in contact with the wall. The same configuration was used in [11] to validate a finite element method for various Navier-Stokes-Cahn-Hilliard (NSCH) models. In the present paper, we extend this problem to 3D, assuming an axisymmetric shape which is realistic according to experimental observations in the considered regime [12].

The paper is organized as follows: Sect. 2 describes the numerical approach for the simplified model employing an immersed boundary method (IBM) and the NSCH

model for the original problem. The model with agglomerates, a Navier-Stokes-Cahn-Hilliard-Surface-Phase-Field-Crystal model (NSCHSPFC) will only be considered in 2D. Section 3 gives the benchmark configuration and presents numerical results. Conclusions are drawn in Sect. 4.

2 Numerical approaches

2.1 Phase field model with finite element approximation

We consider a non-dimensional NSCH model of the following form:

$$\rho_r(c)\left(\partial_t \mathbf{u} + (\mathbf{u}\cdot\nabla)\mathbf{u}\right) = -\nabla p + \frac{1}{G}\nabla\cdot(\eta_r(c)\mathbf{D}) + \mu\nabla c + \mathbf{F}, \qquad \nabla\cdot\mathbf{u} = 0, \quad (3)$$

$$\partial_t c + \mathbf{u}\cdot\nabla c = \gamma\Delta\mu, \qquad \mu = \frac{3}{2\sqrt{2}\epsilon Eo}\left(W'(c) - \epsilon^2\Delta c\right). \quad (4)$$

The equations are defined in Ω with c denoting the phase field variable distinguishing between the two fluid domains, $c \approx -1$ inside the bubble and $c \approx 1$ in the surrounding fluid with a smooth transition at the interface. The evolution of the interface is implicitly determined by the evolution of c. The quantity $W(c) = \frac{1}{4}(c^2-1)^2$ defines a double well potential, ϵ a length scale determining the width of the diffuse interface, and γ the mobility. The nondimensional parameters

$$G = \frac{\rho_2\sqrt{|\pi_\rho - 1|\, g\, d^3}}{\eta_2},\ Eo = \frac{|\rho_2 - \rho_1|\, g\, d^2}{\sigma},\ \pi_\rho = \frac{\rho_1}{\rho_2},\ \pi_\eta = \frac{\eta_1}{\eta_2}$$

denote the Galileo number, Eötvös number, density ratio and viscosity ratio, respectively. All quantities in (4)–(7) are dimensionless. The volume-equivalent diameter of a sphere $d = d_{eq}$ serves as the characteristic length and the reference velocity is given by the gravitational velocity $\sqrt{|\pi_\rho - 1|gd}$, yielding a reference time scale of $\sqrt{d\,/\,(|\pi_\rho - 1|g)}$. The relative density and viscosity are determined as a function of c according to $\rho_r(c) = (1+c)/2 + \pi_\rho(1-c)/2$ and $\eta_r(c) = (1+c)/2 + \pi_\eta(1-c)/2$, respectively. The body force $\mathbf{F}$ is the buoyancy force directed upwards of magnitude $\rho_r(c)/(1-\pi_\rho)$.

We consider an axisymmetric formulation and adapt the discretization used in [11]. Let T_h be a triangulation of the 2D domain $\Omega = [0,w]\times[0,l]$ where l is the channel length and w the width of the axisymmetric domain equal to the channel radius. Furthermore, let us partition the time interval $[0,T]$ with step size $\tau := T/M$. We define the discrete time derivative $d_t v^m := (v^m - v^{m-1})/\tau$, where the upper index denotes the time step number. Furthermore, for a non-negative integer j, let $P_j(K)$ denote the space of polynomials of degree less than or equal to j on a triangle $K \in T_h$. We introduce the finite element spaces

$$M_h = \{q \in C^0(\Omega) | q_{|K} \in P_1(K)\}, \quad (5)$$

$$V_h = \{v \in C^0(\Omega) | v_{|K} \in P_2(K), v(x,0) = v(x,l), v(w,y) = 0, \forall (x,y) \in \Omega\}, \quad (6)$$

$$Y_h = \{v \in C^0(\Omega) | v_{|K} \in P_2(K), v(x,0) = v(x,l), \forall x \in [0,w]\}, \quad (7)$$

and denote by $\mathbf{V}_h = (V_h)^2$ the space of 2D test functions. A semi-implicit Euler time-stepping algorithm is used where the Cahn-Hilliard and Navier-Stokes systems are coupled in one linear system. Higher order algorithms for the individual systems are applicable as well (see e.g. [13]). We now introduce a scaled velocity field

$\tilde{\mathbf{u}} = (u_r/r, u_\theta)$, where r is the distance from the symmetry axis, u_r the radial and u_θ the circumferential velocity component. The finite element approximation now reads:

Find $(\tilde{\mathbf{u}}^m, p^m, c^m, \mu^m) \in \mathbf{V}_h \times M_h \times Y_h \times Y_h$ such that for all $(\mathbf{v}, q, \psi, \xi) \in \mathbf{V}_h \times M_h \times Y_h \times Y_h$

$$
\begin{aligned}
(\rho_r(c^{m-1}) d_t \tilde{\mathbf{u}}^m, rB\mathbf{v}) + (\rho_r(c^{m-1}) \tilde{\mathbf{u}}^{m-1} r^3 A \tilde{\mathbf{u}}^m, A\mathbf{v}) + (\rho_r(c^{m-1})(\tilde{\mathbf{u}}^{m-1} \cdot rC\nabla)\tilde{\mathbf{u}}^m, B\mathbf{v}) \\
+1/G(r\eta_r(c^{m-1})(C\nabla\tilde{\mathbf{u}}^m)^T, C\nabla\mathbf{v}) + 1/G(r\eta_r(c^{m-1})\nabla\tilde{\mathbf{u}}B, \nabla\mathbf{v}) - 1/G(r^2 A\nabla c^{m-1}\tilde{\mathbf{u}}^m, A\mathbf{v}) \\
-(p^m, rC : \nabla\mathbf{v} + 2rA\mathbf{v}) - (\rho_r(c^{m-1})\mathbf{g} + \mu^m \nabla c^{m-1}, rC\mathbf{v}) = 0, \\
(rC : \nabla\tilde{\mathbf{u}}^m + 2rA\tilde{\mathbf{u}}^m, q) = 0, \\
(d_t c^m, r\psi) - (\tilde{\mathbf{u}}^m \cdot c^{m-1}, rC\nabla\psi) + (\gamma\nabla\mu^m, r\nabla\psi) = 0, \\
Eo2/3\sqrt{2}(\mu^m, r\xi) - \epsilon(\nabla c^m, r\nabla\xi) - \epsilon^{-1}(W'(c^m), r\xi) = 0,
\end{aligned}
$$

where $A = \left[\begin{smallmatrix} 1 & 0 \\ 0 & 0 \end{smallmatrix}\right], B = \left[\begin{smallmatrix} r^2 & 0 \\ 0 & 1 \end{smallmatrix}\right], C = \left[\begin{smallmatrix} r & 0 \\ 0 & 1 \end{smallmatrix}\right]$, and (f, g) denotes the $L^2(\Omega)$ inner product. We linearize the derivative of the double well potential $W'(c^m)$ by a first-order Taylor series expansion: $W'(c^m) \approx (c^{m-1})^3 - c^{m-1} + (3(c^{m-1})^2 - 1)(c^m - c^{m-1})$. The adaptive finite element toolbox AMDiS [14] is used for discretization. The code has been validated for the 2D implementation against the benchmark problem [10,11] and against experimental results for Taylor bubbles [15].

We use a standard Taylor-Hood element for the Navier-Stokes equation with polynomial degree two for $\mathbf{u}, c, \mu$ and one for p. Adaptive meshes are indispensable for high spatial resolution along the fluid-fluid interface described implicitly by c. While the domain away from the interface is discretized with an equidistant mesh of grid size $h = 0.2$, we used a finer grid at the interface with grid size $h_{int} = 0.0125$ in all our simulations. The resulting meshes are similar to meshes generated by an L^2-like error indicator based on a jump residual (e.g., [14]). Note, that rigorous error estimates in h and ϵ only exist for simpler problems like the Allen-Cahn equation [16]. The model with agglomerates is described in detail in [3,4]. Also in this setting, a standard Taylor-Hood element for the Navier-Stokes equation with polynomial degree two for $\mathbf{u}, c, \mu$ and degree one for p is used, as well as adaptive meshes to resolve the fluid-fluid interface. The additional quantities along the interface, such as the particle density, are discretized using elements of degree one. The mesh size is the same as above.

2.2 Immersed boundary model with finite volume approximation

Simulations were also conducted with an Euler-Lagrange approach. This approach employs a fictitious fluid inside the bubble which has the same properties as the surrounding fluid, with the advantage that no jumps at the phase boundaries need to be resolved. The incompressible Navier-Stokes equations (1) are then solved with the parameters of the surrounding fluid in the domain Ω. The equations are discretized on a staggered grid in Cartesian coordinates employing a second order finite volume method and integrated over time using a Runge-Kutta three-step method with implicit treatment of the viscous terms.

The bubble is represented by the IBM of [17] with the improvements of [18] and extension to non-spherical bubbles [19] as discussed below. The motion of the bubble is determined by solving its linear and angular momentum equation

$$
m_p \frac{d\mathbf{u}_p}{dt} = \oint_\Sigma (\eta_2 \boldsymbol{D} - p\mathbf{I}) \cdot \mathbf{n} \, ds + V_p(\rho_1 - \rho_2)\mathbf{g}, \quad \frac{d\,(\mathbf{I}_p \mathbf{u}_p)}{dt} = \oint_\Sigma \mathbf{r} \times (\eta_2 \boldsymbol{D} \cdot \mathbf{n} - p\mathbf{n}) \, ds, \quad (8)
$$

where $\mathbf{u}_p$ and $\boldsymbol{\omega}_p$ denote the linear and angular velocity of the bubble center, m_p and $\mathbf{I}_p$ designate its mass and tensor of inertia while $\mathbf{n}$ denotes the outward-pointing normal vector of the interface Σ, with $\mathbf{r}$ identifying a vector from the bubble center to a point on Σ. The evaluation of the surface integrals in (8) is obtained from the momentum equation of the background fluid, and the resulting volume integrals are determined efficiently using the signed-distance level set function of the bubble surface [18]. Coupling between the phases is realized by the appropriate body force $\mathbf{F}$ localized at the bubble surface using an approximation of a delta function. To this end, the regularized delta function proposed in [20] is used. It has similar properties as the considered phase-field approximation in the NSCH approach and requires the same high resolution along the interface. Here, however, a globally refined mesh is used with the code employed. The phase boundary is represented by a set of discrete surface markers. Seeding of forcing points on the bubble surface is performed by surface triangulation. If the bubble shape is constant, e.g. spherical, this approach avoids the delicate computation of surface tension via discretization of the curvature. If variations in the bubble shape are to be included, the bubble shape is approximated as an oblate ellipsoid of aspect ratio $X = a/b$ with semi-axes $a = c > b$. During the ascent, the shape of the ellipsoidal particle is modified over time according to a correlation for its aspect ratio X based on the instantaneous bubble Weber number $\mathrm{We} = \rho_2 \, |\mathbf{u}_p|^2 \, d/\sigma$. To this end, the time-averaged data in [21] were fitted by the relation $X^{-1}(t) = 1 - 0.75 \tanh(0.1556 \, \mathrm{We}(t))$ which is also employed for the correlation between the instantaneous bubble velocity and the aspect ratio X. This approach avoids evaluation of local curvature terms. Also, the bubble volume is conserved exactly due to the analytic description of the bubble shape as an ellipsoid.

An additional difference from the NSCH model is the boundary condition (BC) at Σ. As already motivated above and supported by [22], a no-slip BC is applied. This reduces the coupling of the flow inside the bubble to the surrounding flow, with continuity of the derivative still being required.

The simulations reported below were performed with a fully parallel 3D implementation based on domain decomposition for the continuous phase and master-slave communication for the dispersed bubble phase. The in-house code PRIME [23] used here has been validated against experimental and numerical data for heavy and light solid particles [18], as well as for high Reynolds number bubbles in liquid metal [22].

2.3 Comparison

Table 1 gives an overview of the modeling and numerical components of both approaches. The phase field description can handle general two-phase flow problems including topological changes. The IBM employs an ellipsoidal shape for the bubble and consequently can simulate only single or multiple bubbles. This can be relaxed as discussed above and coalescence has recently been implemented, but is not used here. Although the NSCH approach conserves the global volume of the phase field, conservation of the bubble volume can not be assured. The NSCH method is used with a finite element method (FEM) on adaptive, unstructured grids and a semi-implicit Euler time-stepping. The IBM is based on the finite volume method (FVM) using a fixed Cartesian grid and semi-implicit Runge-Kutta time-stepping. A 2D axisymmetric discretization is employed with AMDiS, while PRIME works in 3D. A 3D version of AMDiS exists, but is not employed here for reasons of efficiency. An axisymmetric version of PRIME does not exist.

Table 1. Overview of differences between the methods employed.

	NSCH	**IBM**
two phase model	general	solid particles, bubbles
bubble representation	phase field method	immersed boundary method
flow	in both fluids	in both fluids
bubble deformation	by surface tension	ellipsoidal bubble model
space discretization	FEM	FVM
time discretization	semi-implicit Euler	semi-implicit Runge-Kutta,
grid	adaptive, unstructured	fixed, Cartesian
volume loss	possible	conserved
domain	2D axisymmetric	3D

Table 2. Numerical parameters used in the simulations.

	NSCH	**IBM**
step size of spatial discretization	$h = 0.2$ in the bulk $h = 0.0125$ at the interface	$h = 0.025$
time step	$\Delta t = 0.0025$	$\Delta t = 0.0022$
viscosity ratio	$\pi_\eta = 0.1;\ 1.0;\ 10.0$	—
other parameters	$\gamma = 0.0005, \epsilon = 0.01$	—

3 Benchmark configuration and results

The 3D liquid domain is given by $\Omega = [0, 6.4] \times [0, 12.8] \times [0, 6.4]$ with periodic BCs for all variables in all directions. For NSCH the corresponding cylindrical domain is used with periodic BCs at the top and bottom boundary and no-slip BCs at the side walls. A circular bubble of diameter $d = 1$ is initially placed in the center of the domain. The parameters $G = 170$, $\pi_\rho = 0.5$ were selected for all simulations and two Eötvös numbers were considered: (a) a basically spherical bubble: $Eo = 0.5$, (b) a deformable bubble: $Eo = 5.0$. For the NSCH simulations a viscosity ratio $\pi_\eta = \eta_1/\eta_2$ has to be specified. We therefore subdivide cases (a) and (b) each into three cases: (1) $\pi_\eta = 0.1$, (2) $\pi_\eta = 1.0$, (3) $\pi_\eta = 10.0$. Table 2 gives an overview of the parameters used for the two different approaches. Note, that the NSCH model requires resolution of the steep gradients of the phase-field variable at the interface. This is accounted for by using an adaptive grid with a fine resolution at the interface. For the IBM, a fine grid of constant step size was used in the whole domain. A constant time step was used, yielding a CFL number below 0.3 for the time interval computed.

3.1 Results

The simulations were run until the final time $T = 11$, which corresponds to approximately one crossing of the domain. Therefore no interaction of the bubble with its own wake is expected. No steady flow is reached at this stage. While the IBM conserves mass exactly, the bubble loses up to 2% of its volume in the NSCH simulations. A suitable quantity to use for comparing the computed solutions is the rise velocity reported in Fig. 1 by the corresponding Reynolds number. Another issue is the shape of the bubble, quantified by the circularity, which is defined here as

$$\text{circularity} = \frac{\text{perimeter of area-equivalent circle}}{\text{perimeter of bubble}}$$

using a 2D slice through the bubble center normal to the z-axis.

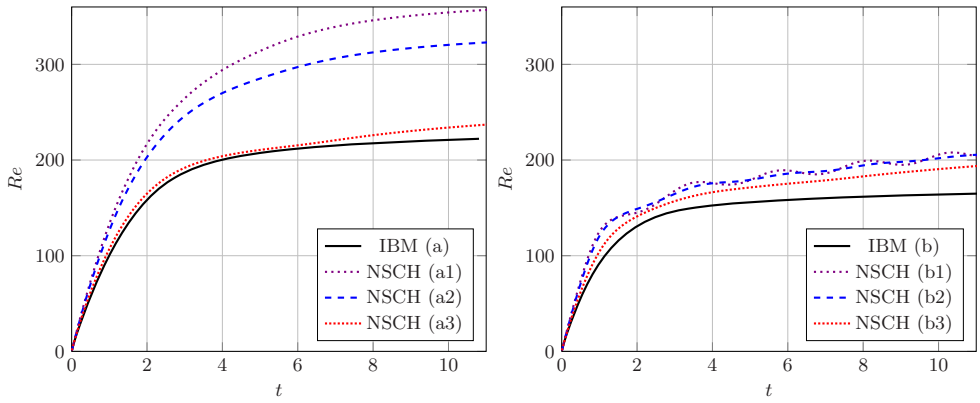

Fig. 1. Rise Reynolds number $\mathrm{Re} = v_p d/\eta_2$ over time. Left: case (a) $Eo = 0.5$, Right: case (b) $Eo = 5.0$. Cases a1, b1 as well as a2, b2 and a3, b3 refer to $\pi_\eta = 0.1,\ 2.0,\ 10$, respectively.

For the spherical bubble ($Eo = 0.5$), the viscosity ratio alters the rise velocity, yielding larger values for small viscosity inside the bubble. For $\pi_\eta = 10$, this configuration approximately matches the case of a solid sphere imposed with the IBM until $t = 6$, with slight deviations for $t > 6$. Note that the IBM was validated for solid particles [18]. For lower viscosity ratios, the initial acceleration of the bubble is larger with NSCH. This is expected because of the higher drag in the IBM simulations due to the no-slip BC. The differences in the rise velocity are more pronounced for smaller bubble viscosities (a1,b1) and decrease for higher bubble viscosities (a3,b3). This seems reasonable, since the higher viscosity makes the bubble stiffer so it behaves more like a solid and thus mimics the no-slip BC.

The bubble shape also has an influence on the rise velocity. For the spherical bubble (a) the influence of the viscosity ratio seems to be higher than for a deformable ellipsoidal bubble (b). In test cases (b1) and (b2) small oscillations of the bubble velocity appear in the NSCH simulations, which is consistent with the benchmark results in [10]. These oscillations can neither be seen in the IBM simulation, nor in NSCH with higher bubble viscosity (b3).

The bubble shapes for Test Case (a) are not displayed here, since the bubble remains spherical in both codes due to the high surface tension. For Test Case (b) Fig. 2 gives an impression of the bubble shape sliced along the xy-plane through the bubble center. The ellipsoidal model used with the IBM seems to approximate the bubble shape quite well. This can be further investigated by looking at the circularity depicted in the same figure. More distinctive shape oscillations occur in the NSCH simulations, in particular for Test Case (b1). These oscillations are significantly reduced by increasing the bubble viscosity (b2, b3). A comparison of the circularity suggests convergence of the two approaches with increasing viscosity.

We now compare the velocity profiles at the bubble center for Test Case (a) displayed in Fig. 3. With the IBM approach, the flow field inside the bubble has very little influence on the bubble shape, its rise velocity or the flow field outside. In the NSCH simulation, these issues are all coupled, and the velocity at the interface is not equal to the rise velocity of the bubble.

The velocity at the interface significantly differs between the models. With the IBM approach, the bubble velocity is equal to the velocity at the bubble boundary in the case of a non-rotating and non-deforming bubble. This is not true for the NSCH approach and is approximated only for high viscosity ratios. All differences observed between the models result from this discrepancy.

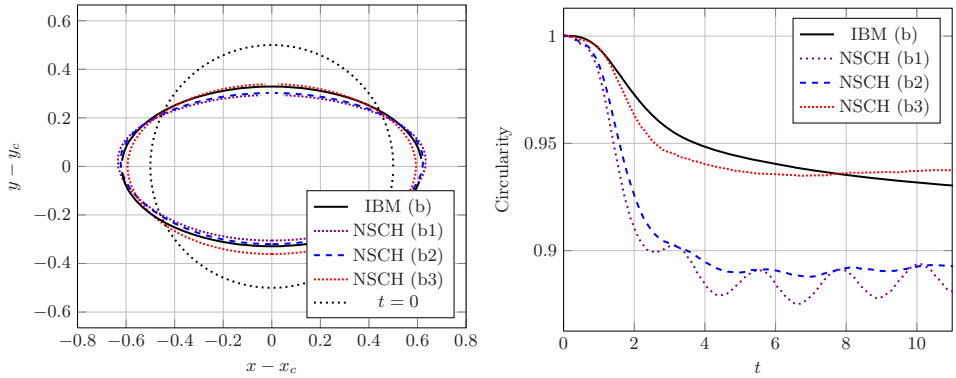

Fig. 2. Evolution of bubble shape for $Eo = 5$, case (b) $Eo = 5.0$. Right: Circularity over time. Left: Bubble shape at final time $T = 11$.

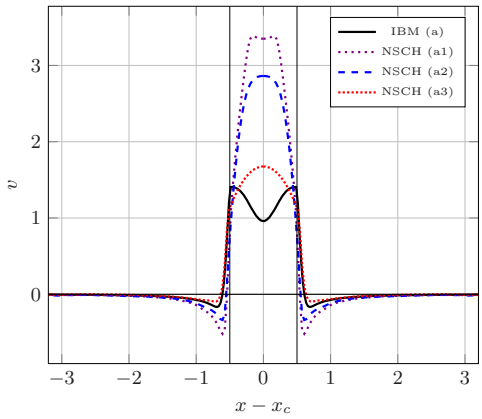

Fig. 3. Velocity profiles at the bubble center, $y = y_c$, at final time T for Test Case (a). The vertical lines indicate the bubble boundary.

As the last comparison, we therefore consider the extended NSCHSPFC model which accounts for the agglomerates. These simulations are only possible in planar 2D due to the available implementation. We compare the approach with the NSCH equations, now also considered in 2D. The parameters remain as for Test Case (a). Figure 4 shows the bubble rise velocity and velocity profile for a clean bubble, named NSCH (a2), a particle-laden bubble of same viscosity, named NSCHSPFC (a2), and a clean bubble with a ten times higher viscosity, NSCH (a3). The rise velocity shows a very good agreement between the particle-laden bubble and the highly viscous bubble. Both rise slower than the clean bubble (NSCH (a2)), confirming that the agglomerates slow down the rise velocity.

The velocity profiles outside of the bubble shown in Fig. 4 (right) provide further support. They are almost identical for the particle-laden and the highly viscous bubble. The fluid velocity is almost constant inside the particle-laden bubble. This implies that the fluid velocity at the bubble boundary equals the bubble velocity, which corresponds to a no-slip condition. Thus, the simulation results with the agglomerates using the NSCHSPFC model correspond to results of the NSCH model with a highly viscous bubble, which indeed can be modeled as a solid particle with no-slip BC.

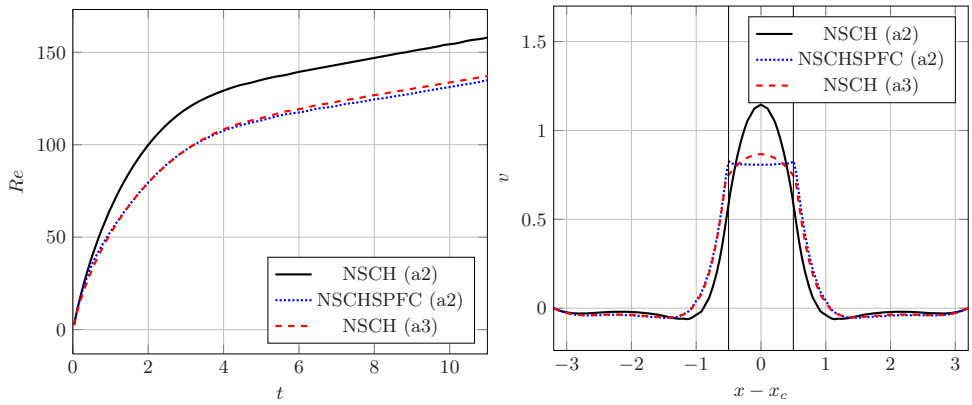

Fig. 4. Rise Reynolds number $\mathrm{Re} = v_p d/\eta_2$ over time (left) and velocity profile at final time (right). The vertical lines indicate the bubble boundary.

3.2 Computational cost

The NSCH approach is more general, more versatile and employs adaptive discretization. It is hence acceptable that the costs per grid point is larger than for the simpler IBM approach. The adaptive discretization of the axisymmetric, hence 2D NSCH system led to an average value of 50,000 degrees of freedom (DOF) for fully coupled NSCH equations. This results in a total runtime of about $8h$ on a single core PC (2.4 GHz).

Computations with the IBM code were run in parallel on 32 CPUs of an SGI Altix. The pressure p and velocity field $(u,\ v,\ w)$ of the continuous phase were determined on a 3D Cartesian grid with 33.6 million cells. The immersed bubble was described by three DOF with respect to translation, three DOF with respect to rotation, and one DOF describing the shape, i.e. the aspect ratio of the oblate ellipsoid. A CPU-time of 32×12.2 CPU hours was used for a single simulation independent of Eo (average of the two runs including I/O), with 95.5% of the time used for the 3D flow field describing the continuous phase and 4.5% for IBM routines.

4 Conclusions

Physical modeling based on experimental information may lead to drastic simplification of numerical models, which then allow for 3D simulation with realistic parameters. The approximations are physically sound and are justified for the specific configuration. However, without numerical benchmarks, such approaches could prevent the algorithm from producing accurate solutions for a general class of problems. For the specific problem of liquid metals, we motivate a drastic model approximation and quantitatively compare the results for a single bubble rising in quiescent fluid obtained with two different numerical algorithms. The NSCH approach considers a two-phase flow model with surface tension and jump BCs at the interface. The IBM approach assumes the bubble to be solid-like and imposes a no-slip condition at the interface. Shape deformations are incorporated by a phenomenological ellipsoidal model depending on the bubble Weber number. Both approaches agree for large surface tensions when a high viscosity ratio is employed to account for the agglomeration of oxides at the bubble surface. In the limit of infinite bubble viscosity, the original two-phase flow model essentially mimics a solid particle and so the very similar results

are not surprising. For a low surface tension and a high viscosity ratio, the ellipsoidal model yields almost the same shape as the full two-phase flow problem. Even for a low viscosity ratio, the difference in the circularity is below 5%. Thus, concerning only the circularity, the phenomenological ellipsoidal model is valid for a wide range of viscosity ratios and surface tensions. For the rise velocity, this is no longer the case. For a low viscosity ratio, the discrepancy between the models cannot be compensated by adjusting the surface tension. The simulation results of the NSCHSPFC model, which directly incorporates the agglomerates at the interface, show a clear difference to the NSCH model with adjusted surface tension. This is in agreement with the results of [24] where it was demonstrated that particle-laden interfaces behave significantly different from interfaces with surfactants, which only have an effect on the surface tension. Agglomerates at the interface show behavior similar to a two-phase flow with a highly viscous bubble. The rise velocity decreases and the fluid velocity at the interface approaches the velocity of the bubble. This can be approximated as a solid particle with no-slip BC, as used with the IBM approach. Thus, agglomerates at the interface indeed highly simplify the original model, enabling large scale simulations with high accuracy.

This work was funded by SFB 609, projects A9 and C10.

References

1. S. Osher, R. Fedkiw, *Level Set Methods and Dynamic Implicit Surfaces* (Springer, 2003)
2. T. Kunugi, S. Satake, Y. Ose, H. Yoshida, K. Takase, *Large Scale Computations in Nuclear Engineering: CFD for Multiphase Flows and DNS for Turbulent Flows with/without Magnetic Fields* (Springer, 2008)
3. S. Aland, J. Lowengrub, A. Voigt, Phys. Fluids **23**, 062103 (2011)
4. S. Aland, J. Lowengrub, A. Voigt, Phys. Rev. E **86**, 046321 (2012)
5. S. Frijters, F. Gunther, J. Harting, Soft Matter **8**, 6542 (2012)
6. R. Bel Fdhila, P. Duineveld, Phys. Fluids **8**, 310 (1996)
7. J. Magnaudet, I. Eames, Ann. Rev. Fluid Mech. **32**, 659 (2000)
8. S. Heitkam, S. Schwarz, J. Fröhlich, Magnetohydrodyn. **48**, 313 (2012)
9. T. Kempe, J. Fröhlich, J. Fluid Mech. **709**, 445 (2012)
10. S. Hysing, S. Turek, D. Kuzmin, N. Parlini, E. Burman, S. Ganesan, L. Tobiska, Int. J. Numer. Meth. Fluids **60**, 1259 (2009)
11. S. Aland, A. Voigt, Int. J. Num. Meth Fluids **69**, 747 (2012)
12. R. Clift, J. Grace, M. Weber, *Bubbles, Drops, and Particles* (Dover Publications, 1978)
13. K. Teigen, P. Song, J. Lowengrub, A. Voigt, J. Comput. Phys. **230**, 375 (2010)
14. S. Vey, A. Voigt, Comput. Vis. Sci. **10**, 57 (2007)
15. S. Aland, A. Hahn, F. Klingbeil, M. Weismann, S. Weller, Int. J. Num. Meth. Fluids (submitted) (2012)
16. X. Feng, H.J. Wu, J. Scientific Computing **24**, 121 (2005)
17. M. Uhlmann, J. Computational Phys. **209**, 448 (2005)
18. T. Kempe, J. Fröhlich, J. Computational Phys. **231**, 3663 (2012)
19. T. Kempe, S. Schwarz, J. Fröhlich, Academy Colloquium Immersed Boundary Methods: Current Status and Future Research Directions, Amsterdam, The Netherlands (2009)
20. A. Roma, C. Peskin, M. Berger, J. Comput. Phys. **153**, 509 (1999)
21. E. Loth, Int. J. Multiphase Flow **34**, 523 (2008)
22. S. Schwarz, J. Fröhlich, 7th Int. Symp. on Turbulence and Shear Flow Phenomena (Ottawa, Canada, 2011)
23. T. Kempe, J. Fröhlich, 8th International ERCOFTAC Symposium on Engineering Turbulence Modelling and Measurements (Marseille, France, 2010)
24. S. Aland, A. Voigt, Coll. Surf. A **413**, 298 (2012)